Experiments in Fluids (2006) 40: 643–653
DOI 10.1007/s00348-005-0104-7

RESEARCH ARTICLE

S. Loose · H. Richard · J. Bosbach · M. Thimm
W. Becker · M. Raffel

Optical measurement techniques for high Reynolds number train investigations

Received: 22 October 2005 / Revised: 15 December 2005 / Accepted: 17 December 2005 / Published online: 10 January 2006

Abstract This article reports on experimental aerodynamic investigations on a generic high-speed train configuration performed within two different wind tunnels. Both wind tunnels are specialized facilities for high Reynolds number investigations and offer low turbulence levels. The wind tunnels are the cryogenic wind tunnel located in Cologne (KKK) and in the high-pressure wind tunnel located in Göttingen (HDG). Both facilities are part of the German–Dutch wind tunnel association (DNW). The adaptation and application of three optical measurement techniques for such high Reynolds number investigations is described in the article. The optical methods are: Particle Image Velocimetry for the measurement of velocity fields, Background Oriented Schlieren technique for density gradient measurements, and a white light Digital Speckle Photography technique for model deformation monitoring.

Keywords High-speed train · PIV · BOS · Digital speckle photography · Leeward vortex

List of Symbls

α	Yawing angle (°)
ω_x	Vorticity (s^{-1})
Γ	Circulation ($m^2\ s^{-1}$)
M	Model scale (1)
U_∞	Free stream velocity ($m\ s^{-1}$)
x, y, z	Coordination system (m)
u, v, w	Velocity components ($m\ s^{-1}$)
T	Fluid temperature (°K)
l	Reference length (m)
P_0	Static wind tunnel pressure (bar)
Re	Reynolds number (1)
Ma	Mach number (1)
v	Kinematic viscosity ($m^2\ s^{-1}$)
ρ	Fluid density ($kg\ m^{-3}$)

S. Loose · H. Richard · J. Bosbach · M. Thimm · M. Raffel (✉)
Deutsches Zentrum für Luft- und Raumfahrt (DLR), Institut für Aerodynamik und Strömungstechnik, Bunsenstraße 10, 37073 Göttingen, Germany
E-mail: Markus.Raffel@dlr.de

W. Becker
Deutsch Niederländische Windkanäle (DNW), Business Unit GUK, Linder Höhe, 51147 Köln, Germany

1 Introduction

Due to the high costs and a limited feasibility of complex laser measurements at full-scale test conditions, most experimental studies on the aerodynamics of high-speed trains are conducted at sub-scale in wind tunnel facilities. However, in most cases both the Reynolds and Mach numbers of the model investigations do not match the full-scale vehicle. Most modern low-speed wind tunnels reach appropriate Mach numbers of $0.1 < Ma < 0.3$. However, if the air speed relative to the train are approximately the same for both the model and the full-scale train, then the Reynolds number in the wind tunnel will be much less than that for a full-scale vehicle in the ratio M of the model- to full-scale dimensions. For aerodynamically well-designed configurations, the resulting mismatch in Reynolds number leads to a certain discrepancy of the location where transition to turbulent flows occurs. This problem is well known from the large number of aeronautical applications related, e.g., wings in wind tunnels, but can partly be solved by boundary layer tripping.

However, flows around trains are more complex because trains usually have a number of important drag-producing small-scale features, like bogies, pantographs, and gaps between cars. The influences of these items are usually taken into account by an extra charge resulting from experiments and previous investigations when simplified models are used [8, 9]. The flow, therefore, is

significantly dependent on the Reynolds number and the risk of misleading model investigations is much larger. This brings facilities into play, which are specialized for high Reynolds number investigations. Whereas, drag measurements in conventional mid-size low-speed wind tunnels are reported to lead to errors of up to 30% [1], significantly reduced errors are expected to result from tests in high Reynolds number facilities [19]. Results of investigations at different Reynolds numbers are shown in Fig. 1. The measurements have been performed within the same wind tunnel campaign in the cryogenic facility described further below. The influence of the Reynolds number onto the measured drag coefficients in the train coordinate system for different yawing angles can clearly be seen.

In addition to the demand of high Reynolds number facilities for the measurement of drag at conditions without relevant crosswinds, they generate additional important effects on drag and rolling moments of trains and are therefore to be investigated. The high length to width ratio and the required yawing angles lead to the necessity of even larger facilities. One of the effects of a crosswind is the change of aerodynamic drag by up to 50% compared to no-wind conditions. Since high-speed operation of modern trains has additionally been accompanied by a significant reduction in train weight, as a result of better structural design and improved materials, the proper measurement of effects related to crosswind has gained an increased importance because of safety considerations. Interest in this subject has even more increased with the introduction of unpowered and therefore lightweight lead vehicles [6].

The aerodynamic lift acting on the frontal part of the train, together with the side force induced by crosswinds and especially gusts lead to generation of strong, unsteady, and attached vortices on the leeward side of the leading vehicle. This can lead to a strong de-loading of the frontal bogie, especially on the windward side.

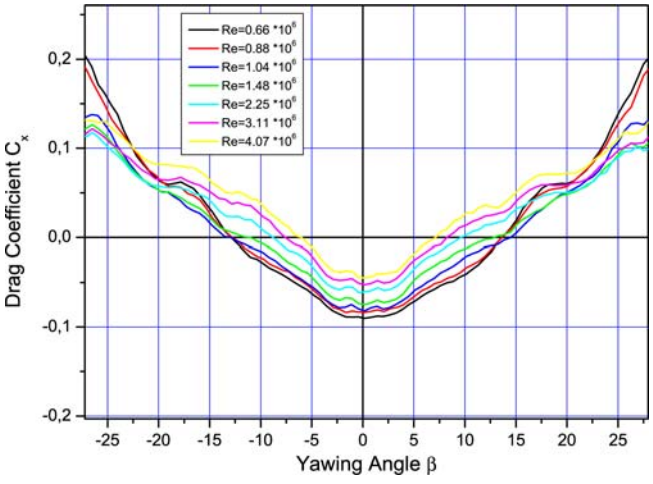

Fig. 1 Drag coefficient for different Reynolds numbers plotted versus yawing angle

In order to achieve an acceptable blockage ratio especially under yawing angles, small models have to be used and high Reynolds numbers can only be achieved by changing the fluid or its viscosity. This can be done in two different ways: either by increasing the pressure of the fluid and/or by decreasing the temperature drastically. The disadvantage of test facilities which can realize pressure increase or temperature decrease is the limited optical access required for laser based measurement techniques and particle seeding issues. Technical solutions for a variety of such problems is described in more detail in the following sections.

2 Facility and model setup: cryogenic wind tunnel DNW-KKK

The cryogenic wind tunnel Cologne (KKK), as shown in Fig. 2, is a closed circuit low speed tunnel with a test section of 2.4 m×2.4 m [17]. To achieve high Reynolds numbers (Fig. 3), the gas temperature in the tunnel circuit can be decreased from atmospheric conditions down to 100°K by injecting and evaporating liquid nitrogen. Around 90 tons of nitrogen are needed to cool the wind tunnel down and 3 kg/s to maintain the fluid temperature at 100°K. The Reynolds number can thus be increased by a factor of 5.5, while the drive power remains constant. Due to the possibility of independent variation of the gas temperature and flow velocity, the influence of the Mach and Reynolds number on the aerodynamic characteristics can be varied independently. (Either Reynolds number variation at constant Mach numbers or vice versa.)

The Reynolds number for model experiments at trains is based on a hydraulic diameter of 3 m in full-scale. The scale of the model was 1:20. The Reynolds number for a high-speed train with a maximum speed of 250 km/h is $Re \approx 10^7$. The half model support was used for the investigation in the KKK wind tunnel. For the first step, a model of a generic high-speed train lead car was refinished and adapted to the balance. The model consists of the front railcar and a wake body downstream which has not been attached to the balance.

All parameters of the model setup, as floor distance and gap width, have been measured repeatedly for the same model. The different repetitions showed nearly identical results. In addition, a detailed study of the influence of the gap width on the drag has been performed in order to ensure realistic conditions concerning the drag coefficient distribution versus yawing angle variation. All later tests were performed at a ground clearance of 0.25 m × $M = 12.5$ mm and a gap width between the model and the rear wake body of ≤ 1 mm.

3 Facility and model setup: high-pressure wind tunnel DNW-HDG

The high-pressure wind tunnel of DNW (HDG), shown in Fig. 4, is a closed circuit low speed wind tunnel, which

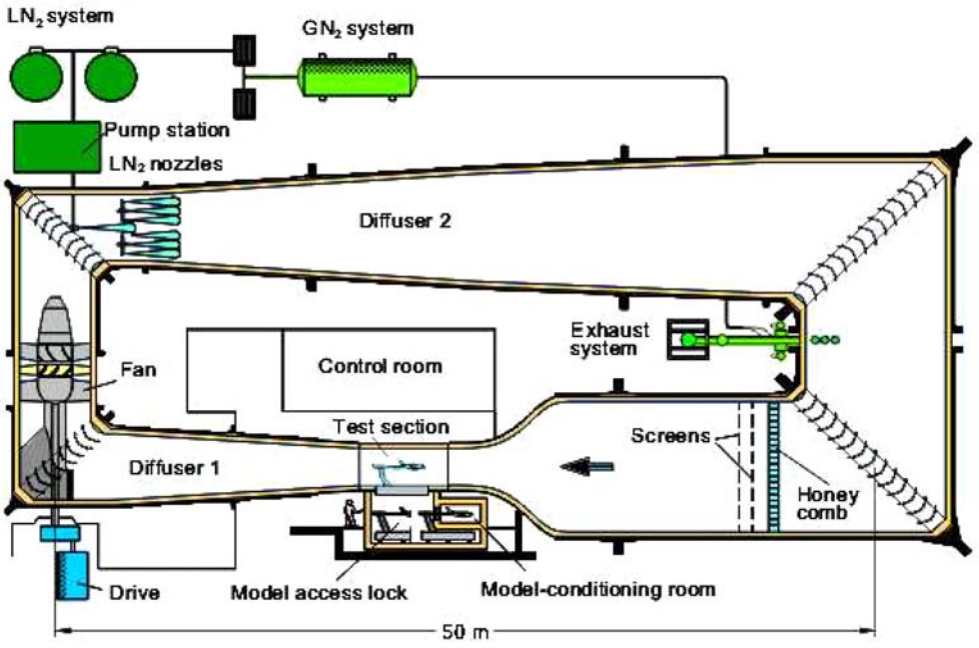

Fig. 2 KKK wind tunnel sketch

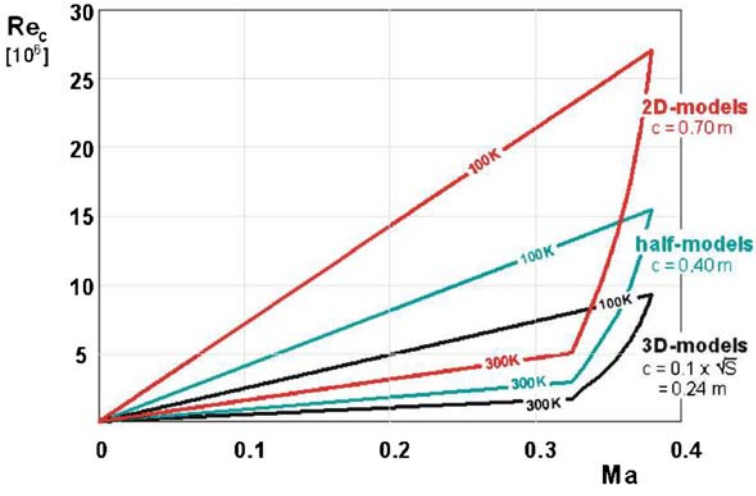

Fig. 3 Covered range of Mach- and Reynolds numbers in KKK

can be pressurized up to 100 bar. The dimensions of the test section are 0.6 m×0.6 m at a length of 1 m. Models 1:50 and 1:66 were used in order to realize a blockage ratio below 10%,. With the maximum speed of 35 m/s and a maximum pressure of 100 bar the achieved Reynolds number was of the same order of magnitude than the full-scale one (e.g., $Re = 10^7$). Figure 5 shows the range of Reynolds numbers that can be obtained depending on the static pressure P_0 in the wind tunnel and free stream velocity U_∞. The flow stays incompressible over the whole range of Reynolds numbers. The model of the lead car and the first part of the trailer shown in Fig. 9 are designed to carry a six-component internal force balance. The strain gage balance is relatively compact and measures forces up to approximately 1,000 N. All components of force and moment are available and have been measured for a range of yaw angles between $-30° < \beta < 30°$ during these tests. The lead vehicle and trailer were mounted sidewards onto the sting.

4 BOS measurements in the cryogenic wind tunnel

In addition to the later described PIV measurements, Background Oriented Schlieren (BOS) visualization, as proposed by Daziel et al. and Raffel et al. [3, 11, 13], has been applied for the first time under cryogenic conditions. This technique allows to visualize rapidly the change of density. The principle of the optical technique can best be compared with the density speckle photography as described by Köpf [7]. In a first step, a reference image is generated by recording a random dot or speckle pattern through air at rest before the experiment. An

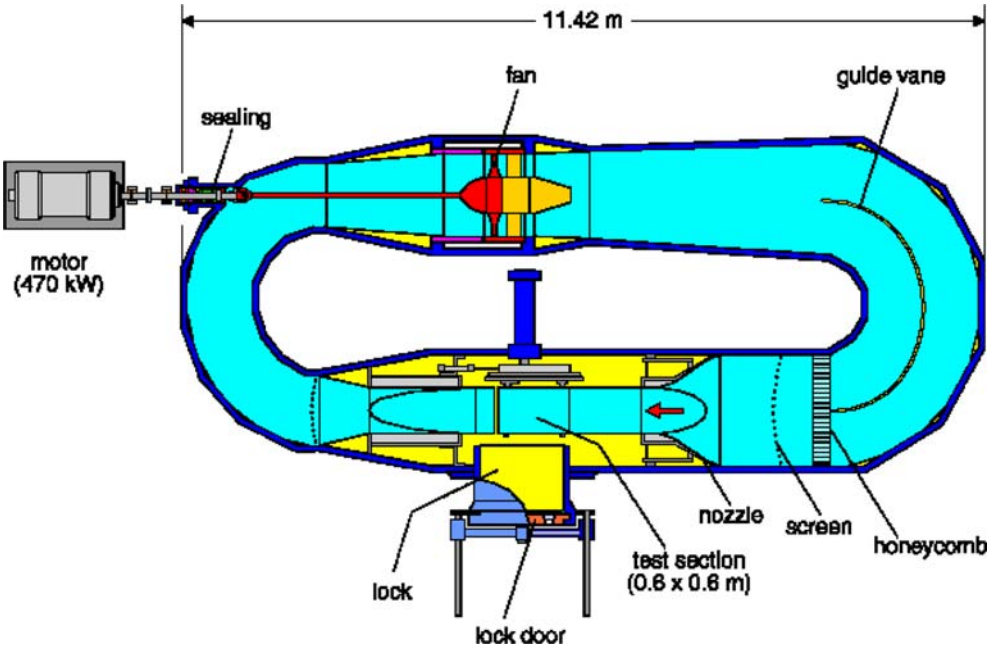

Fig. 4 HDG wind tunnel sketch

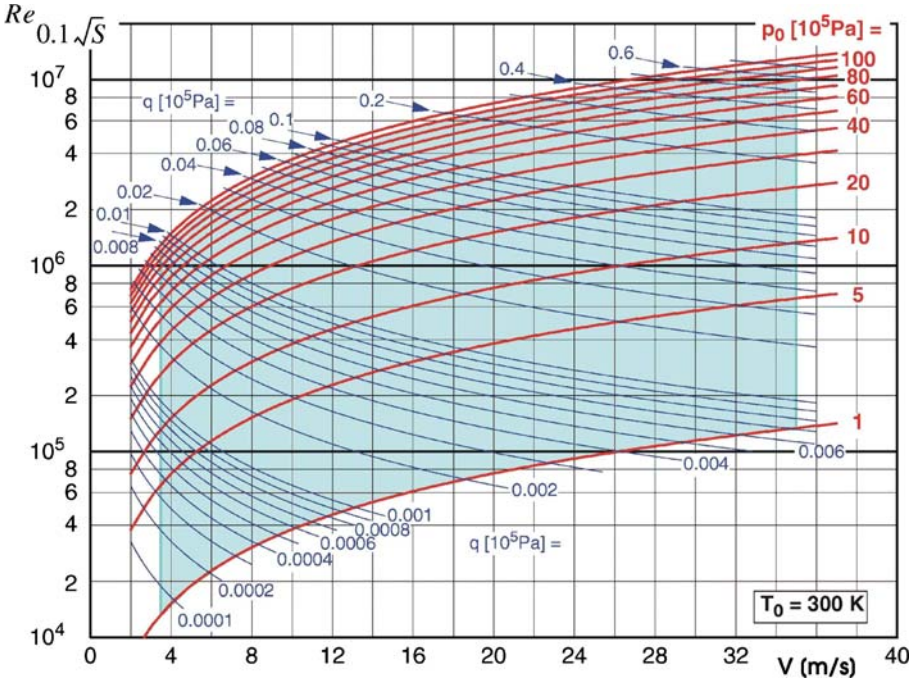

Fig. 5 Covered Reynolds number range in HDG

additional exposure through the flow under investigation (i.e., during the wind tunnel run) leads to a second exposure. The resulting images of both exposures can then be evaluated by correlation methods. In other words, without further evaluation efforts, algorithms which were developed and optimized, e.g., for particle image velocimetry (or other forms of speckle photography), can now be used to determine speckle displacements. It can easily be shown that the deflection of a single beam contains information about the spatial gradient of the refractive index integrated over the optical path (Fig. 6). Assuming paraxial recording and small deflection angles a formula for the image displacement y_i can be derived:

$$y_i = Z_D \times M_i$$

where magnification factor $M_i = z_i/Z_B$ and Z_D = distance dot pattern - density gradient.

The deflection of the beams causes a displacement of the speckle patterns with respect to the patterns of the reference recording, which can be interpreted as density

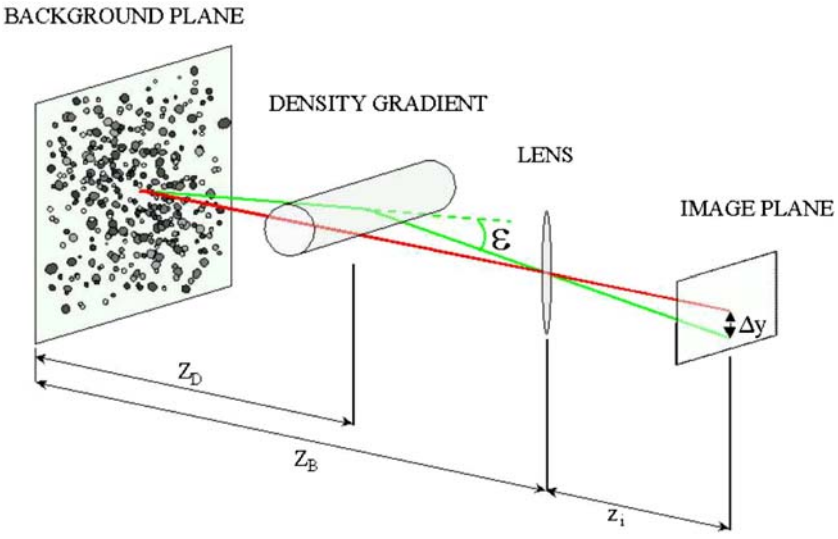

Fig. 6 Principle of the BOS-Technique

gradients, integrated over the optical path, by using the Gladstone-Dale equation. It is obvious that from the two dimensional density gradient an estimate for the density can be derived by integration. After this, the result is comparable to x-ray images and like them, they could be recorded and evaluated in a tomographic manner [13].

The random dot pattern for our investigation was painted on the wind tunnel wall, prior the test (Fig. 7). A reference image was taken at approximately 0.5 m/s wind speed in order to have a homogeneous temperature field in front of the camera and thus avoiding the appearance of density gradients as a consequence of inhomogeneous temperature distributions. A series of 100 images was recorded for each set of parameters during the test. The images were recorded with the same CCD camera that has previously been used for PIV recording. This technique was applied in order to visualize the leeward vortex path. In Fig. 8, the density gradient fields for two different Mach and Reynolds numbers are shown. The density gradients are plotted as vector which point toward the region of lower density inside the leeward vortex. It can be seen that the gradients magnitude is increasing with the Mach number, whereas, the vortex trajectory is very similar for both cases.

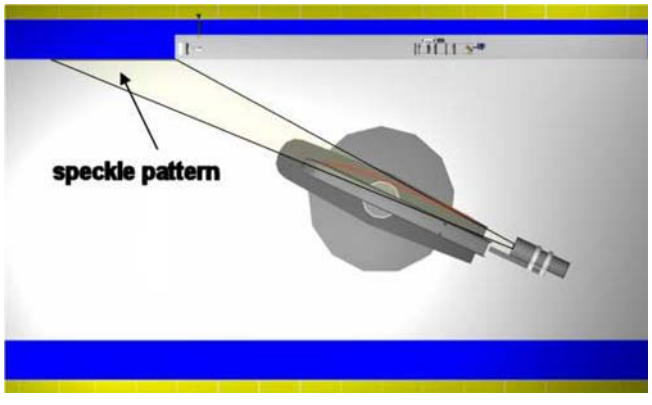

Fig. 7 BOS setup in KKK

Averaged Background Oriented Schlieren results are presented in Fig. 8 for two different free stream Mach numbers: 0.2 and 0.3 for a yawing angle of $\beta = 25°$. It has therefore been demonstrated that the vortex strength and distance from the train can be measured without the need of laser illumination nor the introduction of seed particles in cryogenic facilities. Vortex trajectories can easily be investigated by means of high-speed cameras in order to derive results from unsteady flow features related to vortex separation in future.

5 DSP measurements in the high-pressure wind tunnel

Digital speckle photography (DSP) has been applied to the generic high-speed train models described earlier in order to measure model deflections and deformations due to wind load. The stiffness of models in high-pressure wind tunnels is generally more critical since their dimensions are smaller and the wind loads are higher compared to conventional wind tunnels. DSP is basically an image processing technique that calculates the displacement of a random dot pattern, which is somehow attached or projected onto the object under investigation, by using correlation techniques, just like the previously described BOS technique. The digital correlation algorithms that are used nowadays for DSP, BOS, and PIV are robust and offer small relative errors below 0.1% of full scale. In the case of model deformation measurements presented here, DSP allowed the determination of small deformations with standard deviations of approximately 0.05 Pixel of the CCD camera used. This corresponds to a 1–2 μm accuracy for the measurement of the position of the train model in the HDG wind tunnel. The models, on which a random dot pattern of black ink has been painted, was mounted on a sting and equipped with

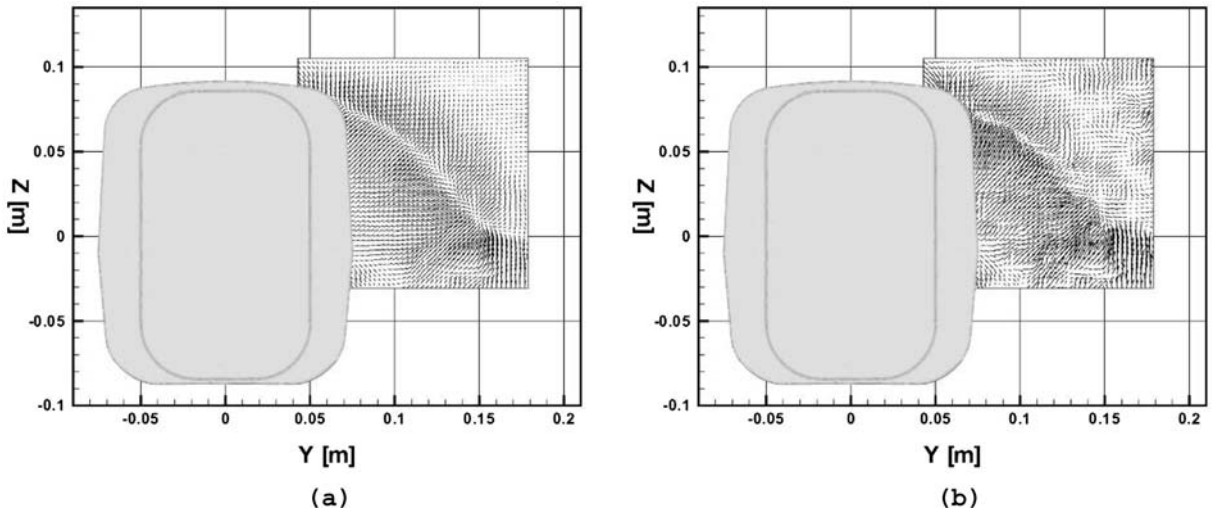

Fig. 8 Vector plots of time averaged density gradients of leeward vortices. $\alpha = 25°$, $T = 100$ K, (**a**) $U_\infty = 45$ m/s, $Ma = 0.2$, $Re = 3.07 \times 10^6$, (**b**) $U_\infty = 63$ m/s, $Ma = 0.3$, $Re = 4.63 \times 10^6$

an internal six component balance (Fig. 9). An additional ground plate was mounted in order to cut off the wind tunnel boundary layer and to ensure defined boundary conditions. The plate was adjusted parallel to the wind tunnel floor by measuring the pressure distribution on the center ($\Delta p = 0$). Only force measurements were performed in the high-pressure wind tunnel, but the white light speckle photography was applied in order to correct the yawing angle. It can easily be seen in Fig. 10 that in spite of the very stiff wind tunnel sting and mounting, the yawing angle of the model was significantly changing depending on the free stream velocity (e.g., 1.3° at 20 m/s).

Figure 10a shows an example of instantaneous white light speckle correlation. One can see the dot patterns painted on the model and the vector field obtained after correlation of the image without flow and the image with flow. One hundred vector fields were used to process the mean averaged angle shown in Fig. 10(b). It can be seen that the displacement increases linearly as a consequence of the sting bending. Additional model deformations, which would result in more complex displacement patterns, have not been observed.

In this way the DSP Technique has been applied here, only deformations in the x–z plane could be measured. In general, this technique is well suited for three-dimensional measurements if two cameras and photogrammetric techniques are used [12].

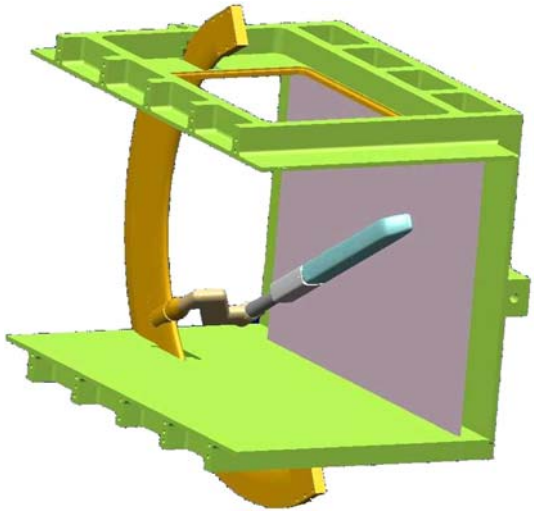

Fig. 9 1:66 scaled model in the HDG test section

6 PIV measurements in the cryogenic wind tunnel

Due to the fact that the test section of the cryogenic wind tunnel is four times larger than that of the high-pressure wind tunnel, a 1:20 scaled model could be used for this PIV investigation. The model did not contain detailed features like bogies, pantographs due to cost reasons. The model was mounted on an additional ground plate (Figs. 11 and 12) in order to create a fresh boundary layer. In addition to PIV, forces and moments were measured with a five components external balance designed for cryogenic conditions. The model was equipped with 46 pressure taps distributed over one longitudinal half of the train. In order to avoid the base pressure induced forces on the train, the front part of a coach was mounted independently from the balance with a gap of 0.8 mm between train and coach.

The PIV setup was a classical 2-C PIV setup as described in reference [10]. It was composed of a 12 bit CCD camera with 1370×1040 px resolution connected to a computer through fiber optic, and a Nd:Yag laser with a maximum energy of 120 mJ per pulse. The camera was equipped with a 50 mm lens with an aperture of 1.4. Figure 11 shows the camera mounted in an electrically heated and thermally insulated box, which was directly

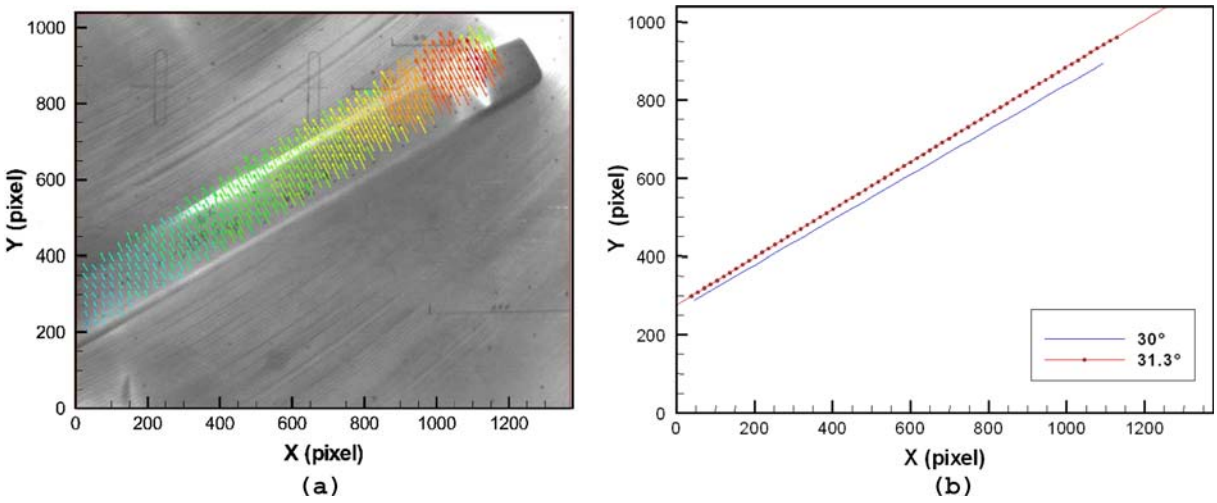

Fig. 10 **a** Instantaneous white light speckle correlation result showing the local displacement vectors color coded by their magnitude. **b** Measured positions of the random dots at a $\alpha = 30°$ reference recording (*blue line*) and the positions measured under wind load at $P_0 = 30$ bar and $U_\infty = 20$ m/s (*red line and dots*)

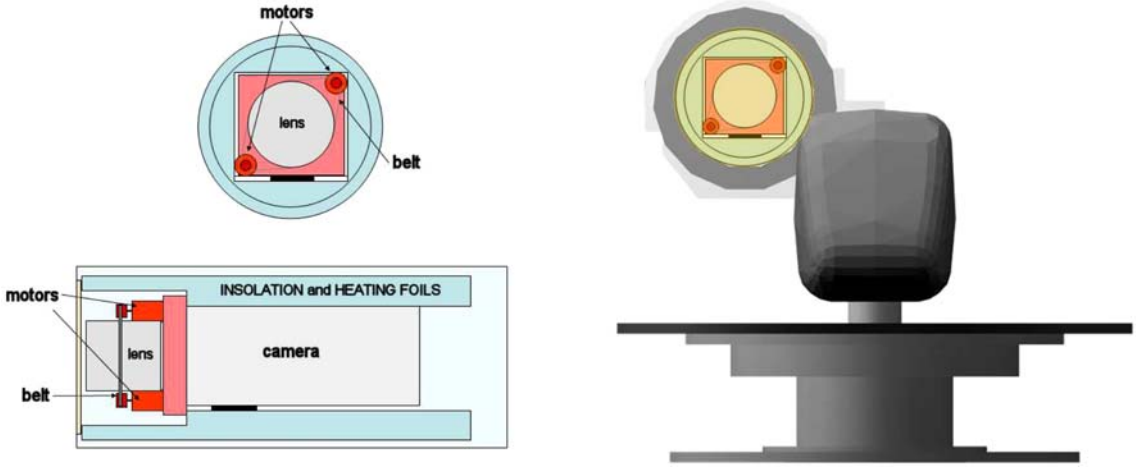

Fig. 11 PIV camera

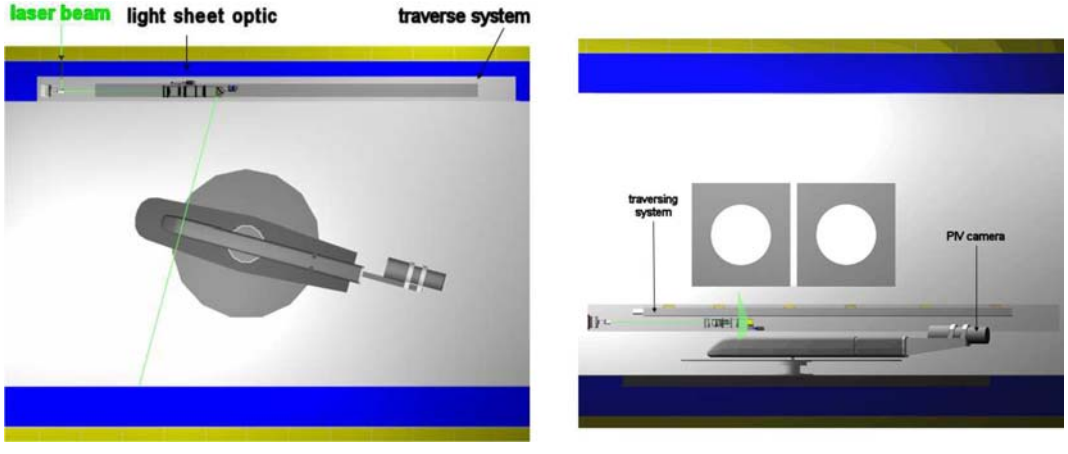

Fig. 12 PIV setup in the cryogenic wind tunnel KKK. The light sheet optics are integrated into the wind tunnel insulation

attached to the end of the coach, parallel to the train. The focus was adjusted using two remotely controlled motors. The front part of the camera box was closed by a 3 mm window glass covered with an electrically heated foil with a maximum power of 1 W/cm^2 in order to avoid refractive index gradients and condensation.

Previous experiments ([14], [2]) showed that the main difficulty was to have a flexible and robust setup which allows to change the position and angle of the light sheet to scan the leeward side of the train model for different yawing angles without the necessity to enter the wind tunnel. Due to the limited optical access through the wind tunnel insulation, the light sheet optics had to be placed within the inner wall of the wind tunnel toward the test section and covered by 6 mm heated glass. The light sheet optics were mounted onto a 3 m remotely controlled traversing system, allowing to scan the complete test section in length. The setup can be depicted in Fig. 12. The laser was installed outside. The laser beam was entering the wall through a hole covered by a glass cylinder. Hot and dry air was blown into the cylinder in order to avoid condensation. A 45° mirror inside the wind tunnel wall was used to couple the laser beam into the light sheet optics.

The light sheet optics mount was especially designed in order to fit within the limited space inside the wall and will be referred to as 'mini-bank' in the following. The light sheet optic was composed of a −60 mm lens to open the laser beam, a 150 mm lens to adjust the light sheet thickness and finally a 80 mm cylindrical lens to generate the light sheet. The mini-bank can be seen in Fig. 13. In order to keep the light sheet thickness constant (between 2 and 3 mm) depending of the yawing angle and of the x-position, the 150 mm lens was mounted onto a small traversing motor equipped with an encoder and with a maximum displacement of 25 mm. A mirror fixed onto a rotating stage was mounted at the end of the mini-bank in order to keep the light sheet always perpendicular to the train model.

The temperature inside the light sheet optics box, inside the camera housing as well as the camera electronic was remotely monitored using thermo-couples and adjusted using heating foils with a maximum power of 0.6 W/cm^2. Prior to the test, the 3 m traverse and the light sheet traverses were carefully calibrated. Because the PIV camera was fixed to the coach of the train, the image magnification was not constant and a calibration grid was recorded at seven different positions as shown in Fig. 14 (left hand side) and linear regression applied in order to obtain the scale factor for every location (right hand side).

Vegetable olive oil was used to generate the particles using several Laskin nozzles in parallel [14]. The nozzles were coupled with a ring impactor in order to ensure that a large amount of particles could be used without any pollution of the insulating material of the cryogenic tunnel by any larger droplets. The particles were injected directly through a 2 m pipe system into the diffuser (Fig. 2). The aerodynamic diameter of the particles was slightly below 1 μm at the exit of the ring impactor. In cryogenic condition, it was observed that the particles scattered more light then in warm conditions. This can partly be explained by the change of refractive index of the fluid as a consequence of the lower temperature. However, a more important role was probably the change of particle state: At 100°K the particles are ice particles which scatter much more light due to the changed shape. This increase of light scattering is an advantage for PIV since it increases the signal to noise ratio.

The setup allowed to scan the complete train model for a large range of yawing angles (from 0° to 45°) but also allowed to save wind tunnel time because only few fractions of a second are necessary in order to change the light sheet location and orientation. The influence of the PIV setup in the model flow field was investigated by measuring forces and moments with and without the PIV setup. It was found that the influence on the overall flow features can be neglected.

A few exemplary results are described below. By increasing the yawing angle of the model, the shear layer on the roof of the model is stimulating a Kelvin-Helmholz instability and rolling up to a vortex sheet [16], whereas, the characteristics of the vortex varied with varying Reynolds number and its position was found to be nearly constant over a wide range of Reynolds numbers ($3\times10^5 < Re < 2.5\times10^6$). Some of the results taken at a Mach number of $M = 0.2$ and a Reynolds number of $Re = 3.07\times10^6$ are shown in Fig. 15. At this point with a yawing angle of $\beta = 17.5°$, the cross-flow area shows a clear shear layer rolling into an vortex, which stays attached to the roof edge of the lead car. At position $x = 400$ mm, the vortex strength is nearly identical but it moved 80 mm further down and 100 mm further away from the lead car.

The existence of this relatively strong and attached vortex in the wake produces additional lift and side forces on the train model. This type of flow structure has been found by various numerical predictions [4] and can be used for more detailed code validation in future. An additional vortex structure developing in the ground flow region has also been observed.

In Fig. 16, the development of the vorticity field on the leeward side of the lead car at position $x = -100$ mm has been shown for increasing yawing angles. It can be seen that the peak vorticity and size of the vortex increases with the yawing angle and that the vortex stays attached to the model. This leads to an increase in vortex circulation. In Fig. 17, the measured side force coefficients for different Reynolds numbers are plotted. It can be seen that only the lowest Reynolds number of $Re = 0.36\times10^6$ investigation shows a certain deviation from the results at high Reynolds numbers. For the higher Reynolds numbers, the coefficients are nearly identical and are symmetric with respect to $\beta = 0°$. The circulation of the leeward vortex at $Re = 3.07\times10^6$ are additionally plotted for different positive yawing angles. It has been found that the circulation distribution at this

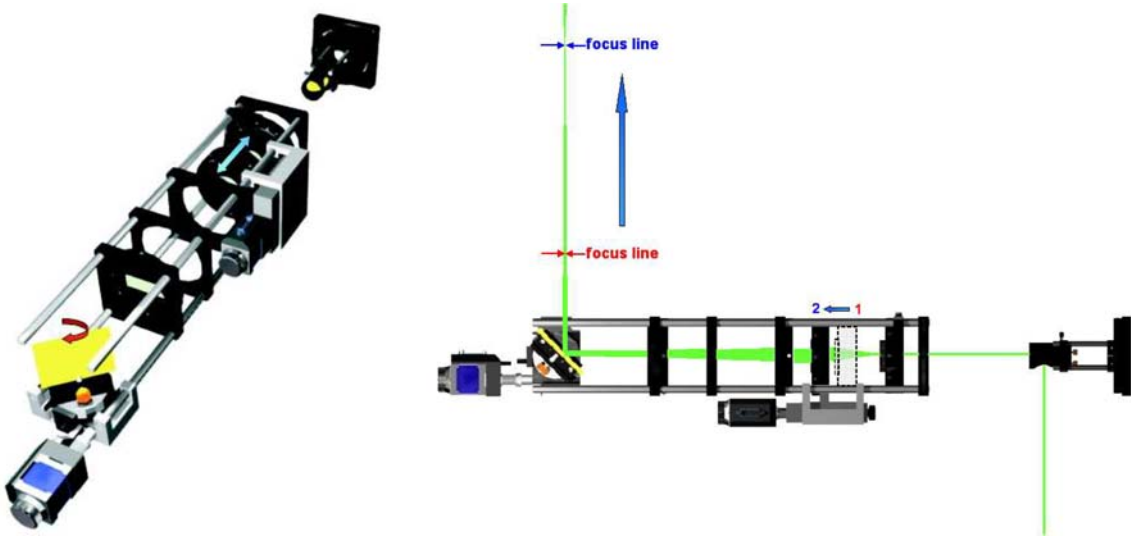

Fig. 13 Light sheet optic

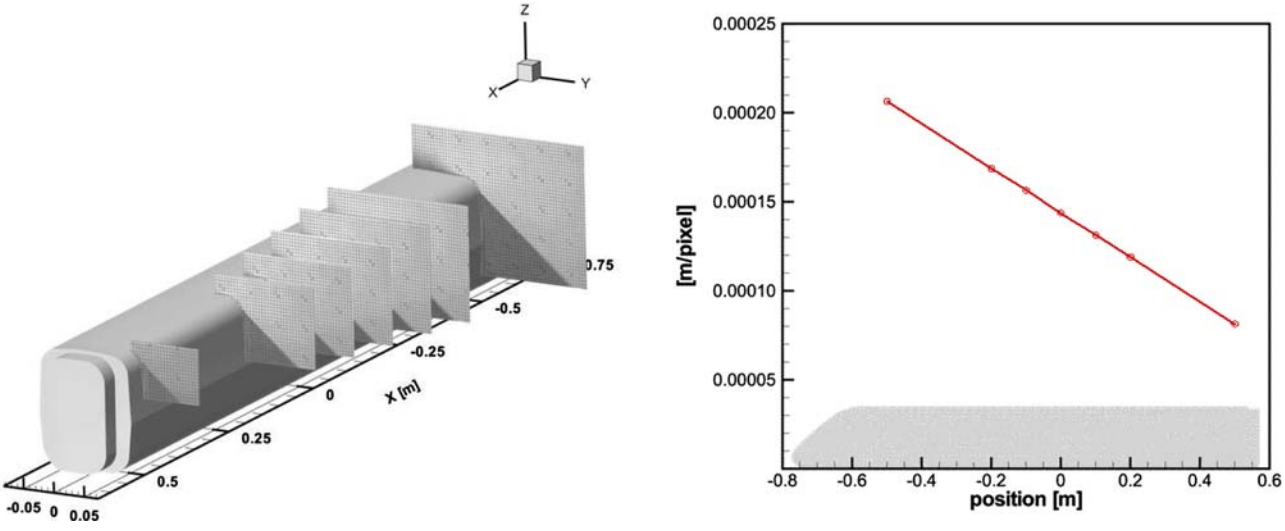

Fig. 14 Perspective view of the calibration grid and calibration curve

position of the model increases proportional to the aerodynamic coefficients and it may be assumed that the effect of flow structures onto the forces can be estimated at least qualitatively from PIV flow field data, especially if the third velocity component will be measured during future tests.

7 Conclusions and outlook

The cryogenic wind tunnel (DNW-KKK) in Cologne and the high-pressure wind tunnel (DNW-HDG) in Göttingen are well suited for ground vehicle aerodynamic investigations, due to the wide range of Reynolds numbers that can be obtained. They have been equipped with different sophisticated optical measurement techniques like PIV, BOS, and DSP for the determination of velocity, density, and deformation fields. An additional interesting feature for detailed aerodynamic investigations of the complex flow fields of ground vehicles is that in spite of the large Reynolds number that can be obtained in the HDG, the Mach number always stays below 0.1 and compressibility effects can therefore be excluded. For future tests, the correlation between optical measurement results and pressure distribution and force measurements is going to be studied especially for the case of unsteady vortex motion, and the interaction between the vortex structure and the vortex induced forces can be studied in more detail and can be used for numerical code validation in future. Stereoscopic PIV will be developed in order to obtain the third velocity component by the angular displacement method.

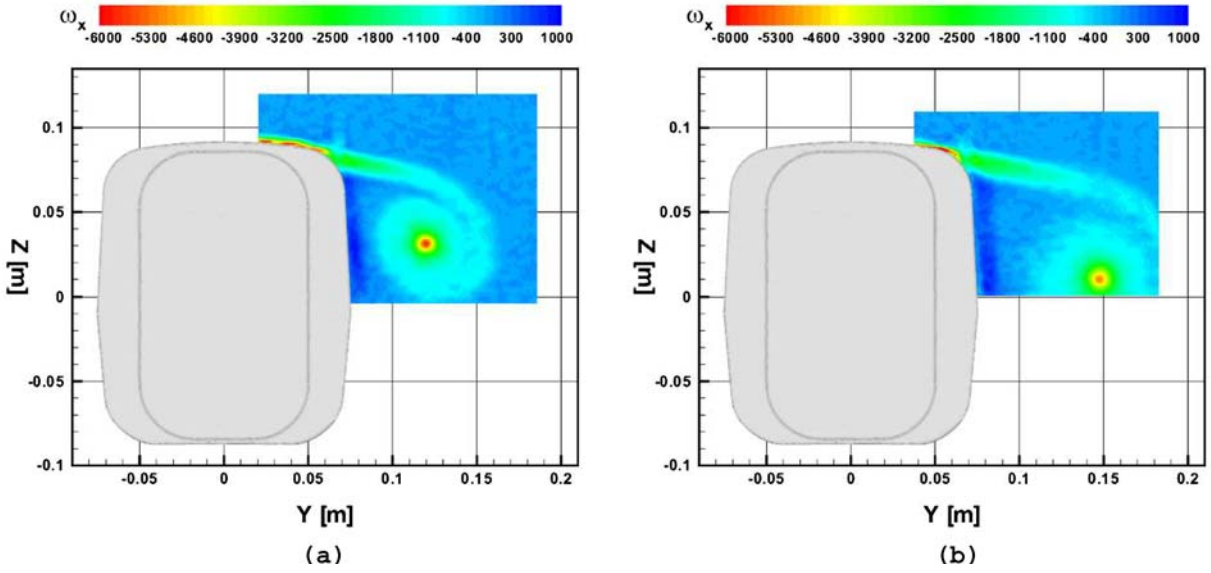

Fig. 15 Averaged vorticity field, $\alpha = 17.5°$, $T = 100$ K, $U_\infty = 45$ m/s, $Ma = 0.2$, $Re = 3.07 \times 10^6$. **a** Position 200 mm. **b** Position 400 mm

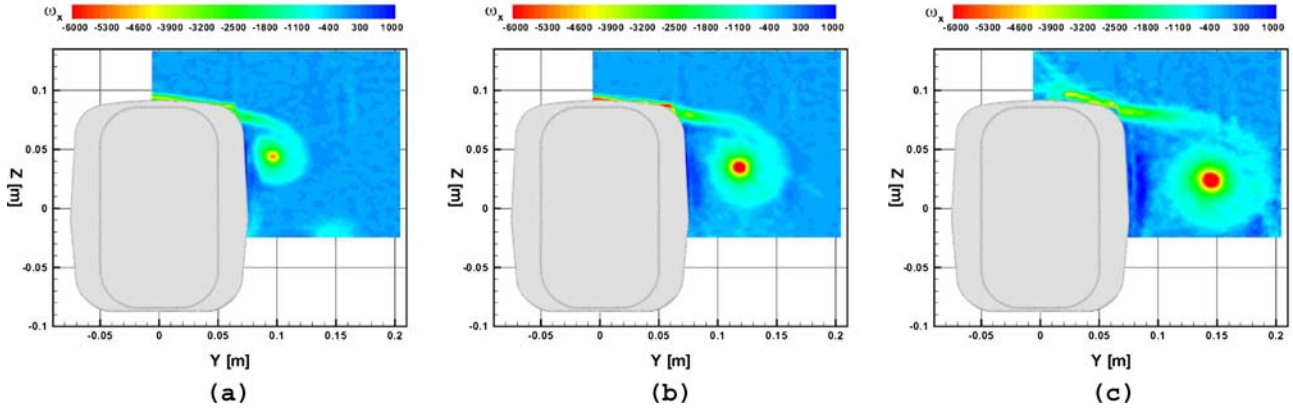

Fig. 16 Averaged vorticity field, position $x = -100$ mm, $U_\infty = 45$ m/s, $Ma = 0.2$, $Re = 3.07 \times 10^6$, $T = 100$ K, (**a**) $\alpha = 17.5°$, (**b**) $\alpha = 25°$, (**c**) $\alpha = 35°$

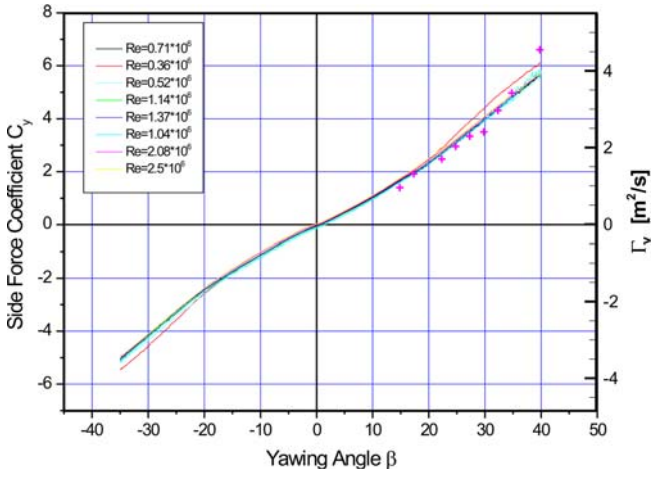

Fig. 17 Side force coefficient (*lines*) and circulation of the leeward vortex (*symbols*) at $Re = 3.07 \times 10^6$ at plotted versus yawing angle

References

1. Baker CJ, Brockie NJ (1991) Wind tunnel tests to obtain aerodynamic drag coefficients: Reynolds number and ground simulation effects. J Wind Eng Ind Aerodyn 38:23–28
2. Becker W, Rebstock R, Loose S, Richard H, Raffel M (2003) Tests for vehicle aerodynamics in the cryogenic wind tunnel cologne DNW-KKK, 20th International Congress on ICIASF, Göttingen, Germany, 2003
3. Dalziel SB, Hughes GO, Sutherland BR (2000) Whole-field density measurements by 'synthetic schlieren'. Exp Fluids 28:322–335
4. Diedrichs B (2003) On CFD modeling of crosswind effects for high-speed rolling stock. In: Proceedings Institution of Mechanical Engineers, vol. 217, Part F: J Train Rapid Transit
5. Ewald B, Viehweger G, Rebstock R (1996) The half-model balance for the cologne cryogenic tunnel (KKK), International Balance Symposium NASA, Langley Research Center
6. Heine C, Matschke G (2002) Full scale tests on side wind effects on trains:evaluations of aerodynamic coefficients and efficiency of wind braking devices. In: Schulte-Werning B, Gregoire R,

Malfatti A, Matschke G (eds) TRANSAERO - A European initiative on transient aerodynamics for railway system optimisation, XIV, 379 pp, Hardcover ISBN: 3-540-43316-3
7. Köpf U (1972) Application of speckling for measuring the deflection of laser light by phase objects. Opt Commun 5(5):347–350
8. Peters JL (1983) Aerodynamics of very high-speed trains and maglev vehicles: state of the art and future potential. Int J Vehicle Design (Special Publication Sp3)
9. Peters JL (1985) Aerodynamische Gestaltung von Schienenfahrzeugen für den Schnellverkehr. Archive für Eisenbahntechnik 40:28–35
10. Raffel M, Willert C, Kompenhans J (1997) Particle image velocimetry, A practical guide. Springer, Berlin Heidelberg New York, 1997, ISBN 3-540-63683-8
11. Raffel M, Richard H, Meier GEA (2000) On the applicability of background oriented optical tomography. Exp Fluids 28:477–481
12. Rastogi PK (2000) Digital speckle pattern interferometry and related techniques. Wiley, New York, 2000, ISBN 0-471-49052-0
13. Richard H, Raffel M, Rein M, Kompenhans J, Meier GEA (2000) Demonstration of the applicability of a Background Oriented Schlieren (BOS) method, In: Proceedings of the 10th International Symposium on applications of laser techniques to fluid mechanics, Lisbon, Portugal
14. Richard H, Becker W, Loose S, Thimm M, Bosbach J, Raffel M (2003) Application of particle image velocimetry under cryogenic conditions. In: 20th International Congress on ICIASF, Göttingen, Germany
15. Stanislas M, Kompenhans J, Westerweel J (1998) Particle image velocimetry, Progress towards industrial application. Kluwer, Dordrecht, 1998, ISBN 0-7923-6160-1
16. Sumantran V, Sovran G (1996) Vehicle aerodyn, SAE Paper ISBN 1-56091-594-3
17. Viehweger G (1989) The Kryo-Kanal Köln (KKK): Description of the tunnel conversion, thermal insulation, instrumentation, operational experience, test results and operating costs, AGARD CP-744, Paper 4
18. Vogt A, Baumann P, Gharib M, Kompenhans J (1996) Investigations of a wing tip vortex in air by means of DPIV. In: Proceedings of the 19th AIAA advanced measurement and ground testing technology, New Orleans, USA,1996, paper AIAA 96-2254
19. Willemsen E (1997) High Reynolds number wind tunnel experiments on trains. Journal on Wind Engineering and Industrial Aerodynamic 6971:437–447